

Improved Algorithm for Multiwavelength Single-Shot Interferometric Surface Profiling: Speeding Up the Multiwavelength-Integrated Local Model Fitting Method by Local Information Sharing

Keisuke Nakata

Tokyo Institute of Technology

2-12-1 O-okayama, Meguro-ku, Tokyo, 152-8552, Japan

`nakata.k.ad@m.titech.ac.jp`

Masashi Sugiyama

Tokyo Institute of Technology

2-12-1 O-okayama, Meguro-ku, Tokyo, 152-8552, Japan

`sugi@cs.titech.ac.jp`

Katsuichi Kitagawa

Toray Engineering Co., Ltd.

1-1-45 Oe, Otsu, Shiga, 520-2141, Japan

`katsuichi_kitagawa@toray-eng.co.jp`

Masafumi Otsuki

Toray Engineering Co., Ltd.

1-1-45 Oe, Otsu, Shiga, 520-2141, Japan

`Masafumi_Otsuki@toray-eng.co.jp`

Abstract

The *local model fitting* (LMF) method is a single-shot interferometric surface profiling algorithm that possesses non-destructive, fast, accurate, and robust measurement capabilities. To extend the measurement range of LMF, extensions based on multiwavelength light sources such as the *multiwavelength-matched LMF* (MM-LMF) method and the *multiwavelength-integrated LMF* (MI-LMF) method were proposed recently. MM-LMF is computationally efficient but it tends to suffer from phase unwrapping errors, whereas MI-LMF tends to be accurate but it is computationally expensive. In this paper, we improve the computational efficiency of MI-LMF by combining it with MM-LMF via *local information sharing*. Through actual experiments, we demonstrate that the proposed method is approximately 10 times faster than the original MI-LMF method, with measurement accuracy kept comparable.

1 Introduction

Interferometric surface profiling allows non-destructive, fast, and accurate measurement of nano-scale surfaces, and thus it is widely used in quality control of various precision industrial products such as semi-conductors and display panels [1].

The *phase shift method* [2] is a classic interferometric surface profiling method that uses multiple fringe images taken by changing the relative phase between the target object and the reference mirror. Although the phase shift method provides high measurement accuracy, it requires a mechanical device such as a piezoelectric actuator to produce fringe images with different relative phases. This makes the measurement apparatus complicated and expensive, and furthermore this causes high vulnerability to external disturbances such as vibration.

To cope with this problem, *single-shot* surface profiling methods such as the *Fourier transform method* [3], the *spatial phase synchronization method* [4], and the *local model fitting (LMF) method* [5] were developed, which require only a single fringe image taken with a tilted reference mirror. The single-shot approach is more robust against vibration and the measurement apparatus is much simpler and less expensive. Among the above single-shot methods, the LMF method was demonstrated to offer highly accurate measurement capability.

The LMF method assumes that the surface of a target object is *locally* flat, and the height of a target point on the surface is estimated based on fringe information in the vicinity. More specifically, a local fringe model is fitted to the observed fringe image by the method of least-squares, which can be analytically performed in a computationally efficient manner. This local measurement principle of the LMF method allows accurate measurement of surface profiles of sharp steps, possibly covered with heterogeneous materials. This is a significant advantage over the Fourier transform method and the spatial phase synchronization method. The *windowed Fourier transform method* [6] also shares similar locality, but it requires the target object to be sufficiently smooth. The *spatial phase shift method* [7, 8] is comparable to the LMF method in terms of the measurement accuracy, but it requires the reference mirror to be tilted exactly to a specified angle, which is hard to achieve in practice. On the other hand, the angle of the reference mirror can be set arbitrarily in the LMF method.

A common weakness of all the above surface profiling methods is that the possible measurement range between neighboring pixels is limited up to a quarter of the light source wavelength, due to the periodicity of single-wavelength light. To extend the measurement range, the *multiwavelength-matched LMF (MM-LMF) method* [9] was proposed, which uses multiple fringe images with different wavelengths such as red, green, and blue. The MM-LMF method is implemented in a novel measurement device that allows single-shot measurement of multiple fringe images with different wavelengths [10]. Therefore, even though multiple fringe images are used, the MM-LMF method is still a single-shot method.

The measurement algorithm of the MM-LMF method consists of the following two stages: First, the plain LMF method is applied to each of the multiple fringe images separately. Note that the LMF solutions have different periodicity because multiple fringe

images have different wavelengths. Then, in the second stage, the LMF solutions obtained from multiple fringe images are matched to find a range-extended solution. Thanks to this simple constitution, the MM-LMF method can be easily implemented and its measurement is computationally efficient. However, under noisy environments, each LMF solution obtained in the first stage become inaccurate and then the matching performed in the second stage can fail. This causes *phase unwrapping errors* and artifacts created by such sporadic phase mismatches degrade the visual quality of the final measurement solution.

To mitigate this problem, the *multiwavelength-integrated LMF (MI-LMF) method* [11] was proposed recently. In the MI-LMF method, a range-extended solution is obtained at once, by simultaneously fitting multiple local fringe models to multiple fringe images. Thanks to this one-shot processing nature, the MI-LMF method can significantly suppress phase unwrapping errors. However, in exchange for the high accuracy, the MI-LMF method requires to solve a non-convex least-squares problem that possesses multiple local optimal solutions. In the original implementation of the MI-LMF method, the global optimal solution is found by exhaustive gradient search from many different initial points, which is computationally very expensive.

In this paper, we propose a new initialization strategy for improving the computational efficiency of the MI-LMF method. Our basic idea is to utilize the MM-LMF solutions in the MI-LMF method. More specifically, we find the global optimal solution by gradient search using the MM-LMF solutions in the *vicinity* as initial points. Through actual measurement experiments, we demonstrate that almost the same measurement accuracy as the original MI-LMF method can be achieved by the proposed initialization strategy, with approximately 90% reduction in computation time.

The rest of this paper is structured as follows. We review the original LMF, MM-LMF, and MI-LMF methods in Section 2. Then, we describe our proposed speeding-up technique and experimentally demonstrate its usefulness in Section 3. Finally, we conclude in Section 4.

2 Review of LMF Methods

In this section, we briefly review the measurement principles of the LMF method [5], the MM-LMF method [9], and the MI-LMF method [11].

2.1 The LMF Method

In the plain LMF method, an interferometric microscope with a single-wavelength light source is employed (Figure 1), where the reference mirror is slightly tilted to introduce spatial carriers. Then an interference pattern at a point (x, y) on the surface of a target object is given as

$$g(x, y) := a(x, y) + b(x, y) \cos \left(\frac{4\pi z(x, y)}{\lambda} + 2\pi px + 2\pi qy \right), \quad (1)$$

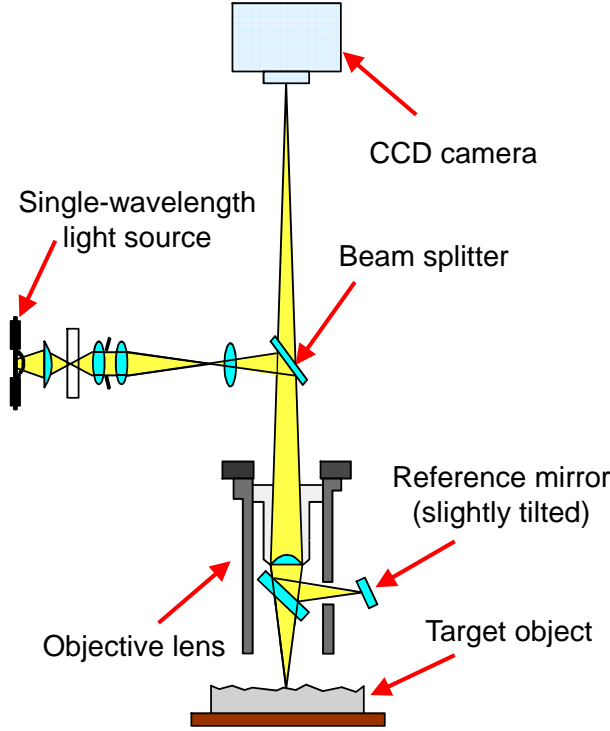


Figure 1: Measurement apparatus for the plain LMF method. In the MM-LMF, MI-LMF, and proposed methods, a multiwavelength light source consisting of red, green, and blue is used.

where $a(x, y)$ and $b(x, y)$ are the bias and the amplitude, $z(x, y)$ denotes the relative height of a target object, λ is the wavelength of a light source, and p and q are spatial carrier frequencies along the x - and y -axes, respectively. We assume that λ , p , and q are known quantities. The goal of the LMF method is to estimate the height $z(x, y)$ from the observed interference image.

In the LMF method, we consider a local area around each target point (x, y) , and assume that $a(x, y)$, $b(x, y)$, and $z(x, y)$ take constant values a , b , and z in the local area, respectively. Then the intensity value at a point (x, y) in the local area is modeled as

$$\bar{g}(x, y) := a + b \cos \left(\frac{4\pi z}{\lambda} + 2\pi p x + 2\pi q y \right), \quad (2)$$

where unknown parameters in this local model are a , b , and z .

After some variable transformations, $\bar{g}(x, y)$ can be equivalently expressed as

$$\bar{g}(x, y) = a + \xi \varphi(x, y) + \zeta \psi(x, y), \quad (3)$$

where

$$\xi := b \cos\left(\frac{4\pi z}{\lambda}\right), \quad (4)$$

$$\zeta := b \sin\left(\frac{4\pi z}{\lambda}\right), \quad (5)$$

$$\varphi(x, y) := \cos(2\pi px + 2\pi qy), \quad (6)$$

$$\psi(x, y) := -\sin(2\pi px + 2\pi qy). \quad (7)$$

Unknown parameters in Eq. (3) are a , ξ , and ζ . To determine these parameters, this local model is fitted to observed intensity values $\{g_i\}_{i=1}^n$ in the vicinity of the target point by the method of least-squares:

$$(\hat{a}, \hat{\xi}, \hat{\zeta}) := \underset{(a, \xi, \zeta)}{\operatorname{argmin}} \sum_{i=1}^n \left(g_i - \bar{g}(x_i, y_i)\right)^2. \quad (8)$$

Thanks to the fact that the local model is linear with respect to a , ξ , and ζ , the least-squares solutions \hat{a} , $\hat{\xi}$, and $\hat{\zeta}$ can be analytically obtained as

$$(\hat{a}, \hat{\xi}, \hat{\zeta})^\top = (\mathbf{A}^\top \mathbf{A})^{-1} \mathbf{A}^\top \mathbf{g}, \quad (9)$$

where $^\top$ denotes the transpose, and \mathbf{A} is the $n \times 3$ matrix and \mathbf{g} is the n -dimensional vector defined by

$$\mathbf{A} := \begin{pmatrix} 1 & \varphi(x_1, y_1) & \psi(x_1, y_1) \\ \vdots & \vdots & \vdots \\ 1 & \varphi(x_n, y_n) & \psi(x_n, y_n) \end{pmatrix} \quad \text{and} \quad \mathbf{g} := \begin{pmatrix} g_1 \\ \vdots \\ g_n \end{pmatrix}. \quad (10)$$

Then we can obtain *candidates* of the target height using $\hat{\xi}$ and $\hat{\zeta}$ as

$$\hat{z}(k) := \frac{\lambda}{4\pi} \arctan\left(\frac{\hat{\zeta}}{\hat{\xi}}\right) + \frac{\lambda k}{2}, \quad (11)$$

where k is an undetermined integer called the *order of interference*. In practice, k is determined by a *phase-unwrapping* algorithm [12], under the assumption that the height difference between two neighboring pixels is less than a quarter of the wavelength λ .

Note that an estimate of the amplitude \hat{b} can also be obtained using $\hat{\xi}$ and $\hat{\zeta}$ as

$$\hat{b} = \sqrt{\hat{\xi}^2 + \hat{\zeta}^2}, \quad (12)$$

which will be utilized later.

Thanks to the local data processing nature of the LMF method, surface profiles of sharp steps possibly covered with heterogeneous materials can be measured accurately in a computationally efficient way. However, a weakness of the LMF method (and all methods that use a measurement apparatus with a single-wavelength light source) is that the measurement range between neighboring pixels is limited up to a quarter of the light source wavelength.

2.2 The MM-LMF Method

To extend the measurement range, the MM-LMF method was proposed [9], which uses multiple fringe images with different wavelengths. Note that the MM-LMF method is combined with a novel measurement device that allows single-shot measurement of multiple fringe images with different wavelengths [10]. This new measurement apparatus has essentially the same structure as the one illustrated in Figure 1, but it uses a *multi-wavelength light source* consisting of red, green, and blue and a *color camera*. Therefore, even though multiple fringe images are used, the MM-LMF method is still a single-shot method.

Suppose multiple interference images for light sources with different wavelengths are observed. Let us denote the intensity value of the j -th fringe image at point (x, y) by $g_j(x, y)$ ($j = 1, \dots, m$). Then $g_j(x, y)$ can be modeled as

$$g_j(x, y) := a_j(x, y) + b_j(x, y) \cos \left(\frac{4\pi z(x, y)}{\lambda_j} + 2\pi p_j x + 2\pi q_j y \right), \quad (13)$$

where $a_j(x, y)$ and $b_j(x, y)$ are the bias and the amplitude of the fringe pattern, λ_j is the j -th wavelength of the light source, p_j and q_j are spatial carrier frequencies along the x -axis and y -axis, respectively. Note that the height of the target object, $z(x, y)$, is common to all $j = 1, \dots, m$. We assume that λ_j , p_j , and q_j for all $j = 1, \dots, m$ are known quantities. The goal of the MM-LMF method is to estimate a surface profile $z(x, y)$ in an extended range from these multiple interference images.

In the MM-LMF method, the plain LMF method is first applied to each interference image to obtain a set of height candidates. According to Eq. (11), the height candidates $\{\widehat{z}_j(k_j)\}_{j=1}^m$ obtained by the LMF method for the j -th fringe image are written as

$$\widehat{z}_j(k_j) := \frac{\lambda_j}{4\pi} \arctan \left(\frac{\widehat{\zeta}_j}{\widehat{\xi}_j} \right) + \frac{\lambda_j k_j}{2}, \quad (14)$$

where k_j is the order of interference for the j -th fringe image. Then the orders k_1, \dots, k_m are determined so that the following *matching error* of $\{\widehat{z}_j(k_j)\}_{j=1}^m$ is minimized:

$$(\widehat{k}_1, \dots, \widehat{k}_m) := \operatorname{argmin}_{(k_1, \dots, k_m)} \left\{ \max[\widehat{z}_1(k_1), \dots, \widehat{z}_m(k_m)] - \min[\widehat{z}_1(k_1), \dots, \widehat{z}_m(k_m)] \right\}. \quad (15)$$

Finally, a range-extended solution \widehat{z} is obtained as

$$\widehat{z} := \frac{1}{m} \sum_{j=1}^m \widehat{z}_j(\widehat{k}_j). \quad (16)$$

Because of the simple constitution of the MM-LMF method, it offers easy and computationally efficient measurement with an extended range. However, due to its two-stage estimation nature, larger errors incurred in the individual LMF solutions obtained in the first stage can cause mismatches of LMF solutions in the second stage. Such mismatches yield *phase unwrapping errors* with peaked artifacts in the final measurement solution, which significantly degrade the visual quality.

2.3 The MI-LMF Method

To overcome the above weakness of the MM-LMF method, the MI-LMF method was proposed recently [11]. The key idea of the MI-LMF method is to fit multiple local models *simultaneously* to multiple interference images. More specifically, suppose that the height $z(x, y)$ is a constant value z in the local area, and the bias $a_j(x, y)$ and amplitude $b_j(x, y)$ in the local area have been estimated as $\hat{a}_j(x, y)$ and $\hat{b}_j(x, y)$, e.g., by the plain LMF method. Then the local model of the MI-LMF method is given by

$$\bar{g}_j(x, y) := \hat{a}_j(x, y) + \hat{b}_j(x, y) \cos\left(\frac{4\pi z}{\lambda_j} + 2\pi p_j x + 2\pi q_j y\right). \quad (17)$$

Note that an unknown parameter in this model is only z , which is estimated by least-squares model fitting using multiple fringe images:

$$\hat{z} := \underset{z}{\operatorname{argmin}} J(z), \quad (18)$$

where

$$J(z) := \sum_{j=1}^m \frac{1}{c_j} \sum_{i=1}^n \left(g_{i,j} - \bar{g}_j(x_i, y_i)\right)^2 \quad (19)$$

is an error criterion, $\{g_{i,j}\}_{i=1,j=1}^{n,m}$ are observed intensity values, and $\{c_j\}_{j=1}^m$ are normalization constants for each wavelength:

$$c_j := \frac{1}{n} \sum_{i=1}^n \hat{b}_j(x_i, y_i)^2. \quad (20)$$

If the amplitude of fringe patterns differs in multiple wavelengths, an image with a larger amplitude will dominate the error criterion (19). To prevent this, the above normalization constants were introduced.

To obtain a range-extended solution, the gradient descent method with multiple initial points is used in the original MI-LMF paper [11]. More precisely, the plain LMF method is first applied to one of the interference images and many height candidates $\{\hat{z}(k)\}_k$ are obtained in some range. Then, the gradient descent method using $\{\hat{z}(k)\}_k$ as initial points is carried out and a set of local optimal solutions, $\{\hat{z}_k\}_k$, is obtained. Finally, the solution \hat{z} that minimizes J is chosen from $\{\hat{z}_k\}_k$.

Because the MI-LMF method contains only a single data-processing step, it can mitigate the occurrence of phase unwrapping errors. However, in exchange for the high accuracy, the MI-LMF method is computationally more expensive than the MM-LMF method because a non-convex least-squares problem is solved by exhaustive multi-point gradient search.

3 Proposed Technique for Speeding-Up the MI-LMF Method

In this section, we explain our idea to speed-up the MI-LMF method and experimentally demonstrate its usefulness.

3.1 New Initialization Scheme for the MI-LMF Method

Our basic idea to speed-up the MI-LMF method is to utilize the MM-LMF solutions as the initial points of the gradient search in the MI-LMF method. If the MM-LMF method has already given a solution with no phase unwrapping error, using that solution as the initial point may give the global optimal solution that minimizes the error criterion (19). However, if the MM-LMF method suffers from a phase unwrapping error, gradient descent from the MM-LMF solution may be trapped by a local optimum.

To overcome this problem, we propose using a *set* of MM-LMF solutions in the *vicinity* of the target pixel as initial points of the gradient search in the MI-LMF method. If there are multiple solutions in the same phase range, we adopt only one of them as the initial point to reduce redundancy. This local information sharing idea is based on the observation that phase unwrapping errors occur only *sporadically*. Thus, even if the MM-LMF method suffers from a phase unwrapping error at the target pixel, at least one of the MM-LMF solutions at its surrounding pixels is expected to contain no phase unwrapping error. Then the global optimal solution may still be obtainable by starting the gradient search from that solution.

If the MM-LMF solutions in the vicinity has high overlap in terms of the order of interference, the proposed method can reduce the number of initial points drastically. Such saving of initial points is directly translated into the reduction in computation time. Later in experiments, we will demonstrate that the number of initial points can be reduced by approximately 90% with this local information sharing scheme.

In the original MI-LMF method, the plain LMF solutions (which are computed from a *single* fringe image) are used as initial points of the gradient search. On the other hand, in the proposed initialization scheme, the MM-LMF solutions (which are computed from *multiple* fringe images) are used as initial points. Because solutions computed from multiple fringe images are more reliable than those computed from a single fringe image, the proposed initialization scheme is expected to improve the quality of each initial point as well. Indeed, we will experimentally demonstrate later that the number of gradient steps until convergence can be significantly reduced by the proposed initialization scheme, which further contributes to saving the computation time.

3.2 Simulation with Artificial Data

Let us numerically illustrate the behavior of the proposed initialization scheme using simulated data and compare its performance with the original MM-LMF and MI-LMF methods.

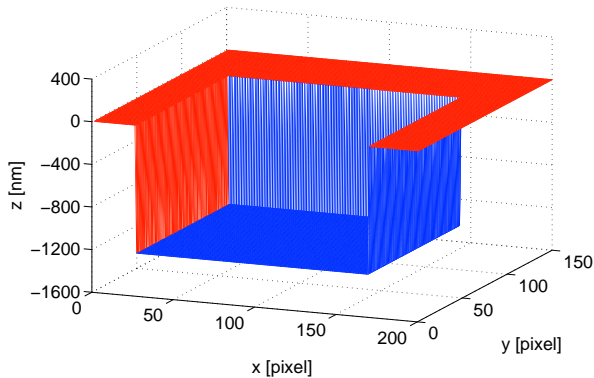
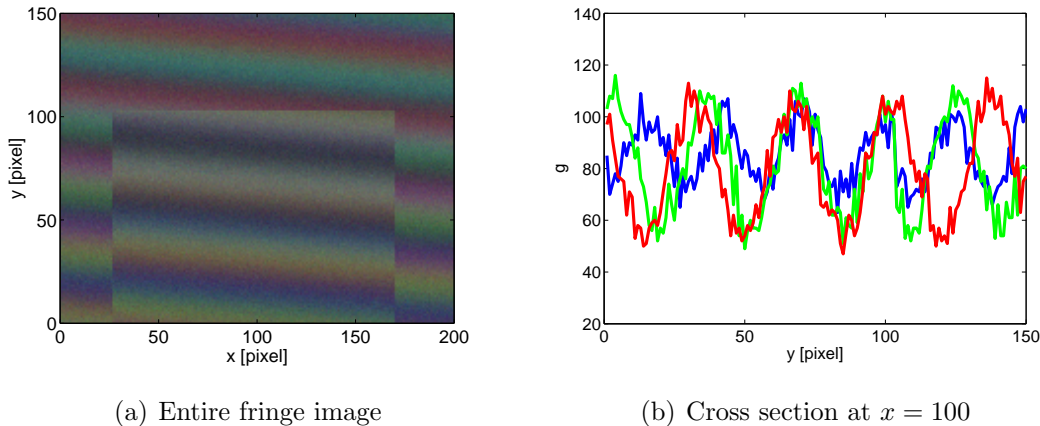


Figure 2: Artificial object.



(a) Entire fringe image

(b) Cross section at $x = 100$

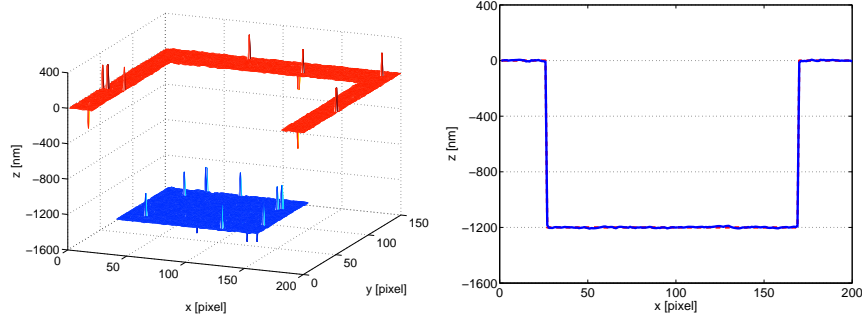
Figure 3: RGB-mixed fringe image for the artificial object.

We set the size of local areas at 3×13 pixels. As estimates of the bias $a_j(x, y)$ and the amplitude $b_j(x, y)$ required in the proposed and original MI-LMF methods, we used the plain LMF solution post-processed by 7×7 -pixel median filtering. We set the vicinity size for local information sharing in the proposed method at 3×3 pixels (see Figure 5(D)).

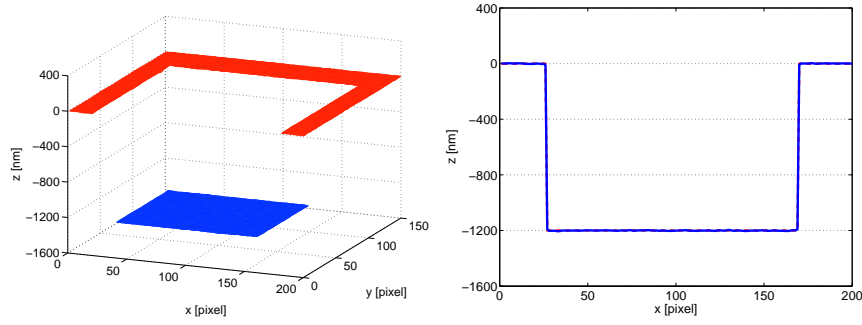
Let us measure the surface profile of the artificial object illustrated in Figure 2. This imitates a color filter used in a flat-panel display, for which we perform actual measurement later. The depth of the hollow is 1200[nm], which is approximately 8–10 times larger than a quarter of the wavelength of visible rays used in standard measurement apparatuses.

Figure 3 shows an observed fringe image for a simulated multiwavelength light source consisting of red ($\lambda_1 = 600$ [nm]), green ($\lambda_2 = 559$ [nm]), and blue ($\lambda_3 = 471$ [nm]). These wavelength choices imitate the actual measurement experiments shown later. For simulating realistic measurements, we added Gaussian random noise with mean 0 and standard deviation 5 independently to each pixel. The size of the fringe image is 200×150 pixels.

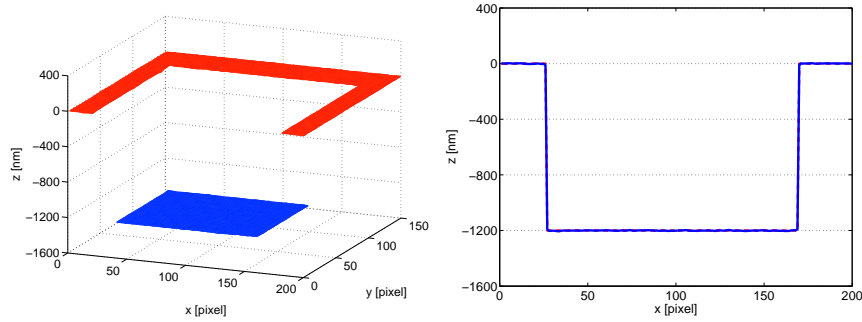
Figure 4 shows measurement results obtained by the MM-LMF, MI-LMF, and proposed methods, where we focused on the flat parts in the top and bottom of the target



(a) MM-LMF



(b) MI-LMF



(c) Proposed Method

	#UE	RMSE	#IP	#GS	CT [sec]
MM-LMF	28	3.41	—	—	6.73
MI-LMF	0	1.70	2.10×10^5	2.86×10^7	417
Proposed Method	0 (0%)	1.70 (0%)	3.79×10^4 (82%)	1.58×10^6 (94%)	32.6 (92%)

Figure 4: Measurement results for the artificial object. Left: 3-dimensional reconstructions. Right: Cross sections at $y = 45$. Bottom: The number of pixels that contain phase unwrapping errors (#UE), the root mean squared error (RMSE) between true and estimated surface profiles at pixels without phase unwrapping errors, the number of initial points for gradient search (#IP), the number of gradient steps (#GS), and computation time for the entire measurement process (CT). Numbers in brackets are reduction rates from the MI-LMF method to the proposed method.

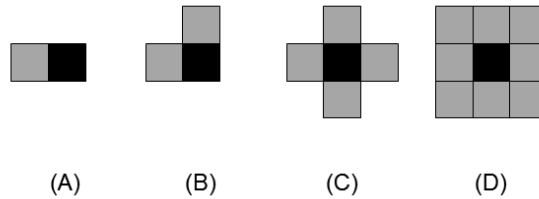


Figure 5: Four choices of vicinity areas for local information sharing. The black and gray square denote the target pixel and vicinity pixels, respectively.

object for better comparison. The number of effective pixels is 20400. The results show that the MM-LMF method tends to suffer from sporadic phase unwrapping errors due to measurement noise, whereas the MI-LMF and proposed methods contain no phase unwrapping error. Moreover, the MI-LMF and proposed methods provide smaller RMSEs than the MM-LMF method thanks to the gradient-based fine-tuning.

Next, let us investigate the improvement in computational costs brought by the proposed local information sharing scheme over the original MI-LMF method. The bottom table in Figure 4 shows that the proposed local information sharing scheme brought approximately 82% reduction in the number of initial points for gradient search and approximately 94% reduction in the number of gradient steps. Thus, the number and the quality of initial points can both be improved by the proposed local information sharing scheme. Consequently, the entire computation time is reduced approximately by 92%.

The performance of the proposed method depends on the choice of the vicinity area for local information sharing. Here we investigate how the performance is affected if the vicinity area is changed. We consider four choices illustrated in Figure 5. Note that the previous experiment (the result reported in Figure 4) corresponds to (D) in Figure 5. The results summarized in Table 1 show that, as the number of vicinity pixels increases from (A) to (D), the estimation accuracy tends to be improved but the computation time grows. (A) is the fastest, but phase unwrapping errors are incurred at two pixels. (B), (C), and (D) produced no phase unwrapping errors and thus (B) is the best choice in this artificial experiment. However, given that the real-world data would be more noisy and improvement of the computation time from (D) to (B) is marginal, we will adopt (D) in the following experiments.

We further evaluate the performance of the proposed method (with vicinity choice (D)) when the surface is tilted or rough. Figure 6 shows measurement results when the top and bottom surfaces have different inclinations (the top surface was tilted as $(0, 0) = 50[\text{nm}]$ and $(200, 150) = -50[\text{nm}]$, and the bottom surface was tilted as $(25, 0) = -1100[\text{nm}]$ and $(175, 100) = -1300[\text{nm}]$). Figure 7 shows measurement results when the surface is rough ($10 \sin(2\pi x/10) + 10 \sin(2\pi y/5)[\text{nm}]$ is added to all pixels). These results show that the proposed method remains effective even if the surface is tilted or rough. Note that RMSEs of the MI-LMF and proposed methods are larger than MM-LMF in Figure 6 because RMSE is computed only at pixels without phase unwrapping errors.

Table 1: Performance of the proposed method for different choices of the vicinity area illustrated in Figure 5. The number of pixels that contain phase unwrapping errors (#UE) and the root mean squared error (RMSE) between true and estimated surface profiles at pixels without phase unwrapping errors are compared in the left half. In the right half, reduction rates of the number of initial points for gradient search (#IP), the number of gradient steps (#GS), and computation time for the entire measurement process (CT) from the MI-LMF method to the proposed method are described.

Vicinity	#UE	RMSE	Reduction Rate		
			#IP	#GS	CT
(A)	2	1.70	85%	95%	94%
(B)	0	1.70	84%	95%	93%
(C)	0	1.70	83%	95%	93%
(D)	0	1.70	82%	94%	92%

3.3 Actual Measurement Experiments

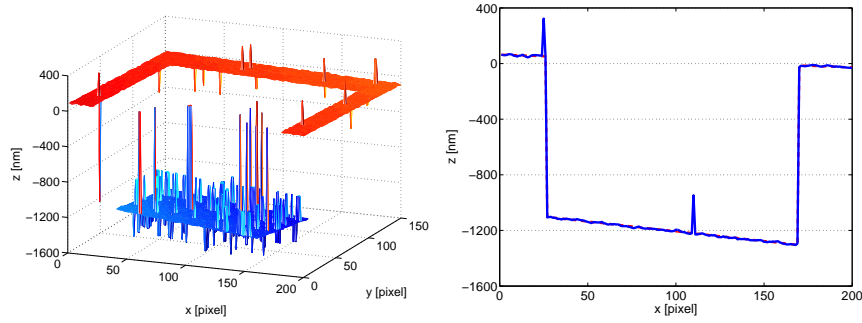
Next, we report the results of actual experiments. We obtained multiple interference images by the multiwavelength single-shot surface profiler *MW-500* developed by Toray Engineering Co., Ltd [10] (see Figure 8). The target object to measure is a color filter for a flat-panel display. This object is expected to have a similar surface profile to the artificial object illustrated in Figure 2, but its true profile is unknown.

Figure 9 show a fringe image obtained by MW-500 with a multiwavelength light source consisting of red ($\lambda_1 = 600[\text{nm}]$), green ($\lambda_2 = 559[\text{nm}]$), and blue ($\lambda_3 = 471[\text{nm}]$). The image size is 200×150 pixels, and each pixel corresponds to $1.28[\mu\text{m}] \times 1.28[\mu\text{m}]$ in actual size.

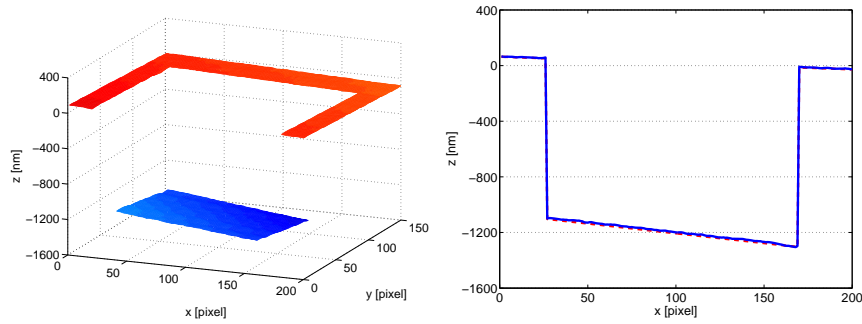
We applied the MM-LMF, MI-LMF, and proposed methods to this RGB fringe image, with exactly the same parameter setup as the previous artificial data experiments. Figure 10 depicts the measurement results of the MM-LMF, MI-LMF, and proposed methods, where the number of effective pixels is 20400. The results show that, although the MM-LMF method tends to suffer from phase unwrapping errors, the MI-LMF and proposed methods can successfully suppress the occurrence of peaked artifacts.

It should be noted that some phase unwrapping errors produced by MI-LMF (Figure 10(b)) are eliminated by the proposed method (Figure 10(c)). This can happened because the global solution of MI-LMF is not necessarily the correct solution in practice due to, e.g., high noise.

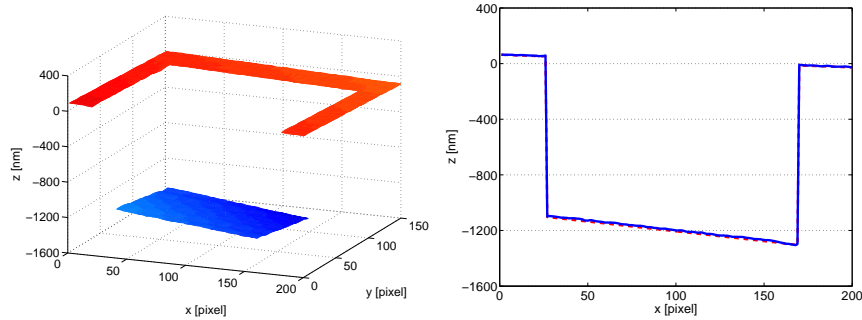
Finally, let us investigate the improvement in computational costs brought by the proposed local information sharing scheme over the original MI-LMF method. The bottom table in Figure 10 shows that the proposed local information sharing scheme brought approximately 78% reduction in the number of initial points for gradient search and approximately 90% reduction in the number of gradient steps. Thus, the number and the quality of initial points can both be improved by the proposed local information sharing scheme. Consequently, the entire computation time is reduced approximately by 88%.



(a) MM-LMF



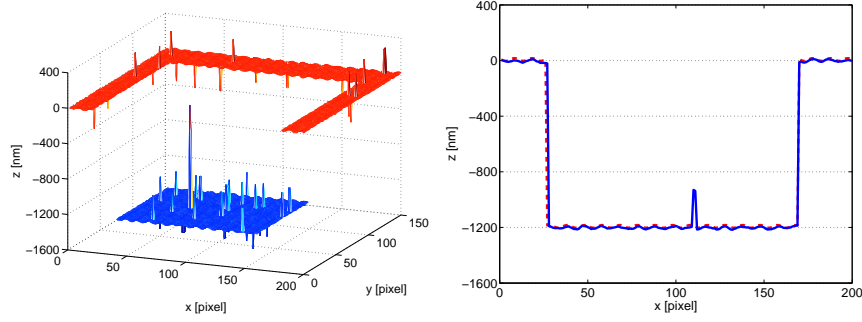
(b) MI-LMF



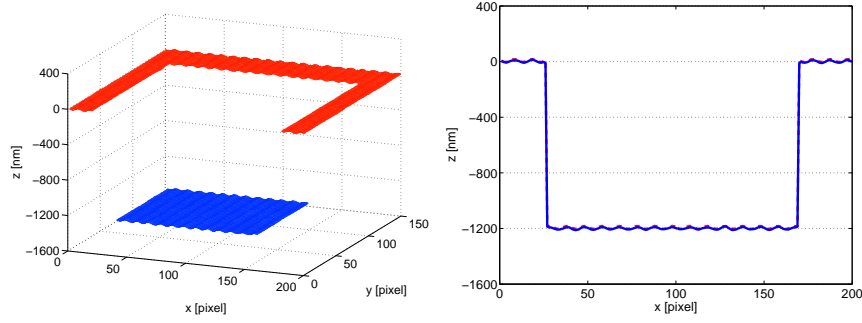
(c) Proposed Method

	#UE	RMSE	#IP	#GS	CT [sec]
MM-LMF	285	4.52	—	—	6.44
MI-LMF	0	6.18	2.10×10^5	2.79×10^7	408
Proposed Method	0 (0%)	6.16 (0%)	3.87×10^4 (82%)	2.37×10^6 (92%)	43.2 (89%)

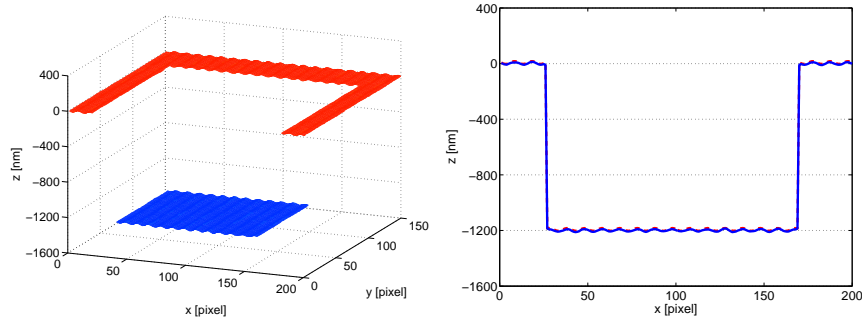
Figure 6: Measurement results for the artificial object with inclinations. Left: 3-dimensional reconstructions. Right: Cross sections at $y = 45$. Bottom: The number of pixels that contain phase unwrapping errors (#UE), the root mean squared error (RMSE) between true and estimated surface profiles at pixels without phase unwrapping errors, the number of initial points for gradient search (#IP), the number of gradient steps (#GS), and computation time for the entire measurement process (CT). Numbers in brackets are reduction rates from the MI-LMF method to the proposed method.



(a) MM-LMF



(b) MI-LMF



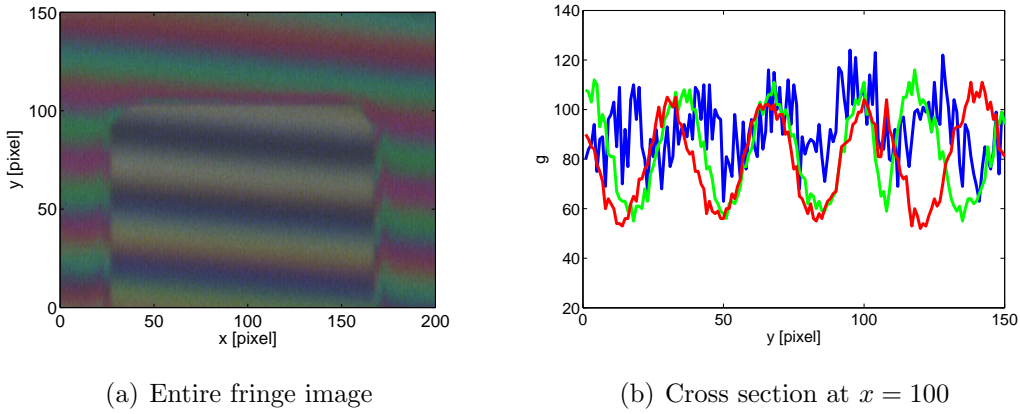
(c) Proposed Method

	#UE	RMSE	#IP	#GS	CT [sec]
MM-LMF	73	8.88	—	—	6.59
MI-LMF	0	6.37	2.10×10^5	2.87×10^7	417
Proposed Method	0 (0%)	6.38 (0%)	4.00×10^4 (81%)	1.84×10^6 (94%)	36.1 (91%)

Figure 7: Measurement results for the artificial object with rough surfaces. Left: 3-dimensional reconstructions. Right: Cross sections at $y = 45$. Bottom: The number of pixels that contain phase unwrapping errors (#UE), the root mean squared error (RMSE) between true and estimated surface profiles at pixels without phase unwrapping errors, the number of initial points for gradient search (#IP), the number of gradient steps (#GS), and computation time for the entire measurement process (CT). Numbers in brackets are reduction rates from the MI-LMF method to the proposed method.



Figure 8: MW-500 developed by Toray Engineering Co., Ltd [10].



(a) Entire fringe image

(b) Cross section at $x = 100$

Figure 9: RGB-mixed fringe image obtained by MW-500.

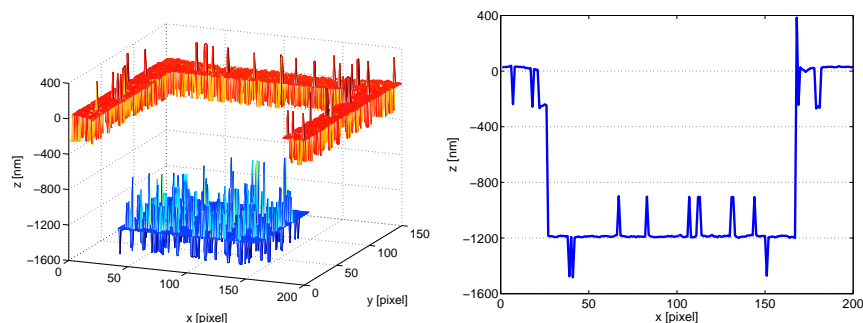
Note also that all the actual measurement results reasonably resemble the simulation results with artificial data in Section 3.2, which substantiates the validity of our artificial data experiments.

Overall, the proposed local information sharing scheme was demonstrated to be a useful alternative to the original MM-LMF and MI-LMF methods.

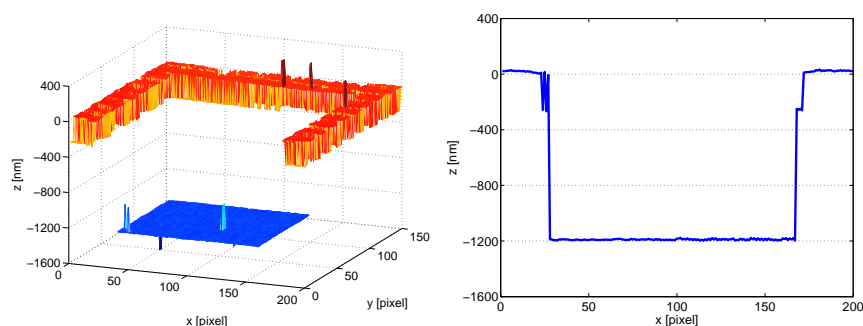
4 Conclusion

The MM-LMF and MI-LMF methods are state-of-the-art multiwavelength single-shot interferometric surface profiling algorithms. The MM-LMF method offers computationally efficient measurement, although it is susceptible to measurement noise and it tends to produce phase unwrapping errors. On the other hand, the MI-LMF method mitigates the occurrence of phase unwrapping errors significantly, even though it is computationally much more expensive due to gradient-based solution search.

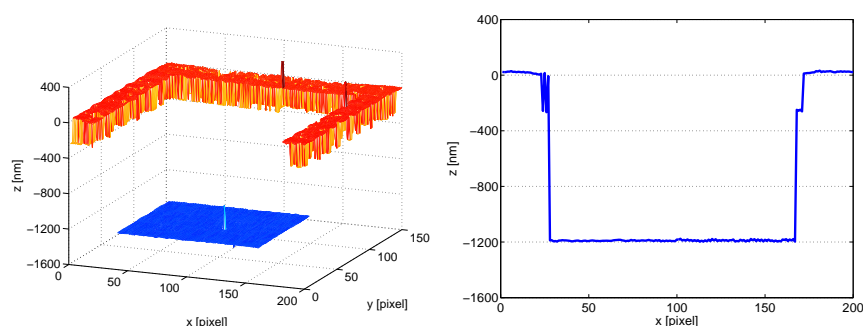
Our contribution in this paper was to combine these two state-of-the-art methods



(a) MM-LMF



(b) MI-LMF



(c) Proposed Method

	#IP	#GS	CT [sec]
MM-LMF	—	—	6.68
MI-LMF	2.10×10^5	3.38×10^7	489
Proposed Method	4.56×10^4 (78%)	3.31×10^6 (90%)	58.3 (88%)

Figure 10: Actual measurement results. Left: 3-dimensional reconstructions. Right: Cross sections at $y = 45$. Bottom: The number of initial points for gradient search (#IP), the number of gradient steps (#GS), and computation time for the entire measurement process (CT). Numbers in brackets are reduction rates from the MI-LMF method to the proposed method.

and to develop a highly practical measurement algorithm. Our key idea was to use the MM-LMF measurement results in the vicinity as initial points for gradient-based solution search in the MI-LMF method, which contributes to reducing the number of initial points and also improving the quality of initial points. Through simulated and actual measurement experiments, we demonstrated that the proposed method retains almost the same measurement accuracy as the MI-LMF method, with approximately 90% reduction in computation time.

References

- [1] S. W. Kim, “High-speed 3D inspection for densely packed semiconductor chips,” (2008). <http://spie.org/x24235.xml?ArticleID=x24235>.
- [2] J. H. Brunning, D. R. Herriott, J. E. Gallagher, D. P. Rosenfeld, A. D. White, and D. J. Brangaccio, “Digital wave front measuring interferometer for testing optical surface and lenses,” *Applied Optics* **13**, 2693–2703 (1974).
- [3] M. Takeda, H. Ina, and S. Kobayashi, “Fourier-transform method of fringe-pattern analysis for computer-based topography and interferometry,” *Journal of Optical Society of America* **72**, 156–160 (1982).
- [4] J. Kato, I. Yamaguchi, T. Nakamura, and S. Kuwashima, “Video-rate fringe analyzer based on phase-shifting electronic moiré patterns,” *Applied Optics* **36**, 8403–8412 (1997).
- [5] M. Sugiyama, H. Ogawa, K. Kitagawa, and K. Suzuki, “Single-shot surface profiling by local model fitting,” *Applied Optics* **45**, 7999–8005 (2006).
- [6] Q. Kemao, “Windowed Fourier transform for fringe pattern analysis,” *Applied Optics* **43**, 2695–2702 (2004).
- [7] D. C. Williams, N. S. Nassar, J. E. Banyard, and M. S. Virdee, “Digital phase-step interferometry: A simplified approach,” *Optics & Laser Technology* **23**, 147–150 (1991).
- [8] N. Brock, J. Hayes, B. Kimbrough, J. Millerd, M. North-Morris, M. Novak, and J. C. Wyant, “Dynamic interferometry,” *Proceedings of SPIE, Novel Optical Systems Design and Optimization VIII*, **5875**, 1–10 (2005).
- [9] K. Kitagawa, “Fast surface profiling by multi-wavelength single-shot interferometry,” *International Journal of Optomechatronics* **4**, 136–156 (2010).
- [10] Toray Engineering Co., Ltd., “MW-500,” (2011). <http://www.scn.tv/user/torayins/>.

- [11] A. Yamashita, M. Sugiyama, K. Kitagawa, and H. Kobayashi, “Multiwavelength-integrated local model fitting method for interferometric surface profiling,” *Applied Optics* **51**, 6700–6707 (2012).
- [12] M. Takeda and T. Abe, “Phase unwrapping by a maximum cross-amplitude spanning tree algorithm: A comparative study,” *Optical Engineering* **35**, 2345–2351 (1996).